Understanding the Impact of Boundary and Initial Condition Errors on the Solution to a Thermal Diffusivity Inverse Problem

by

Xiaojing Fu

Clarkson University

Understanding the Impact of Boundary and Initial Condition Errors on the Solution to a Thermal Diffusivity Inverse Problem

A THESIS BY

Xiaojing Fu

DEPARTMENT OF MATHEMATICS AND COMPUTER SCIENCE

SUBMITTED IN PARTIAL FULFILLMENT OF THE REQUIREMENTS FOR A

Bachelor of Science Degree with

University Honors

April 2011

ACCEPTED BY THE HONORS PROGRAM

Advisor (Kathleen Fowler) Date

Honors Reader Date

Honors Director (Jon Goss) Date

Abstract

In this work, we consider simulation of heat flow in the shallow subsurface. As sunlight heats up the surface of soil, the thermal energy received dissipates downward into the ground. This process can be modeled using a partial differential equation known as the heat equation. The spatial distribution of soil thermal conductivities is a key factor in the modeling process. Prior to this study, temperature profiles were recorded at different depths at various times. This work is motivated by trying to match these temperature profiles using a simulation-based approach and analytic approaches in the context of an inverse problem. Specifically we determine soil thermal conductivities using derivative-free optimization to minimize the nonlinear-least square errors between simulation and data profile. Here, we conduct two sets of studies, assuming homogeneous and heterogeneous soil envrionments respectively. We also study how errors in the initial and boundary conditions propagate over time using both a numerical approach and an analytical method.

Contents

1 Introduction **2**

2 Methodology **2**
- 2.1 Basic Heat Model . . . 2
- 2.2 Estimating Thermal Conductivities . . . 3
- 2.3 Boundary Conditions . . . 4
- 2.4 Initial Conditions . . . 4

3 Parameter Identification Using Optimization **5**
- 3.1 Experimentation on Implementation Details . . . 6
- 3.2 Assumptions on Conductivities . . . 7
- 3.3 Low Amplitude Noise in Top Boundary Condition . . . 8
- 3.4 Using 30cm as Bottom Boundary Condition . . . 8
- 3.5 Time dependent conductivities . . . 10
- 3.6 Bad Data Elimination and Scaled Error Calculation . . . 11
- 3.7 Guided optimization: Error calculation over all time points . . . 12
- 3.8 Summary of Implementation Experiments . . . 14

4 Sensitivity Study On Homogeneous Model **16**
- 4.1 Type I Error . . . 16
  - 4.1.1 Numerical Experiments . . . 17
  - 4.1.2 Analysis and Error Function for Type I Error . . . 18
- 4.2 Type II error . . . 20
  - 4.2.1 Numerical Experiments . . . 21
  - 4.2.2 Analysis and Error Function for Type II Error . . . 23

5 Sensitivity Study on Hetergeneous Model **28**
- 5.1 Type I Error . . . 28
  - 5.1.1 Numerical Experiments . . . 29
  - 5.1.2 Analysis and Error Function for Type I Error . . . 29
- 5.2 Type II error . . . 32
  - 5.2.1 Numerical Experiments . . . 32
  - 5.2.2 Analysis and Error Function for Type II Error . . . 32

6 Conclusion **35**

Acknowledgement

- I would like to thank my advisor and mentor, Kathleen Fowler, for all the encouragement, trust, confidence, freedom, inspiration, honesty, understanding, knowledge, opportunities, emotional support and food that she provided in the past four years. My college would not have been so awesome without you.
- Thank you Brian Leventhal for spending all of those gorgeous summer days with me indoor at concrete cafe. Working on this project with you was pleasant!
- To Dr. Owen Eslinger, thank you for the data and project idea! I have never met you but this is not possible without your support!
- To Dr. Craig, Hayley Shen, Marcy and Clarkson Honors Program, thank you for the wise words, the deadlines and financial support.
- To Clarkson Department of Mathematics and Computer Science, thank you for being the right choice I made.
- And thanks to my parents, Ming Fu and Li Wan, for dealing with me not being home for $\frac{11}{12}$ of the last four years.
- Finally big thanks to my fabulous friends, Akanksha, Allison, Devon, Gabbrielle, Hazelily, Phil, Qian, Ryan and Sam for helping me through the hardest time and for all the good times.

1 Introduction

The one dimensional heat equation is commonly used to model the temperature distribution of a linear heat-conducting system. Knowing the spatially distributed thermal conductivity as well as its initial and boundary temperature, one can approximate the temperature at any given position at any given time in the system. In this study, we are solving the inverse of this problem. Given the initial and boundary condition as well as the temperature profile of the system at all positions and time, our goal is to estimate the thermal conductivities of the linear system.

This work will assist in developing the heat transport capabilities of the three dimensional groundwater and surface water simulator, the **AD**aptive **H**ydrology model, being built by the U.S. Army Corps of Engineers. We will use subsurface temperature data that have been monitored and logged in time and space at a meteorology station. In the given data set, soil temperature is measured at 0cm (top surface), 1cm, 5cm, 10cm, 15cm, 20cm, 25cm and 30cm below the surface and the measurement is taken every 5 minutes for 7 days.

The proposed work will:

- identify, using the data, the best-fit thermal conductivities in the subsurface system;
- analyze how choices made on various aspects of the inverse solution procedure impact the estimation results;
- study the impact of errors in data on the accuracy of estimation

This thesis is outlined in two main parts as follows. In the first part, we began by introducing the general framework for the identification process of thermal conductivities; both analytic method and numerical estimation are considered for the framework, the latter of which will be the focus. Next, we discussed implementation details and challenges of the numerical estimation process and presented results. The second part consists of a sensitivity study of the heat model for both homogeneous and heterogeneous systems. The sensitivity study evaluates how inevitable errors from data impacts the estimation results, thus assisting in determing the reliability of the approximated parameters.

2 Methodology

2.1 Basic Heat Model

The basic model that describes one dimensional, transient heat transport in homogeneous system is shown in Eq.(1):

$$\frac{\partial T}{\partial t} = K \frac{\partial^2 T}{\partial z^2}, \tag{1}$$

where temperature, denoted as T, is a function of time t and space z. The thermal diffusivity is usually referred to as K [L/T] and is related to thermal conductivity by:

$$K = \frac{\hat{k}}{\rho\, c}, \tag{2}$$

where $\hat{k}$ is the thermal conductivity, ρ is the density and c is the heat capacity. Table 1 shows approximate values of thermal diffusivity and conductivity for several materials [1].

Table 1: Approximate values of thermal conductivity and diffusivity of several materials

Material	Aluminum	Copper	Steel	Glass	Concrete	Ice
$\hat{k}\ [\frac{cal}{s\,cm^{\circ}C}]$	0.48	0.92	0.11	0.0014	0.0041	0.004
$K\ [\frac{cm^2}{s}]$	0.83	1.1	0.13	0.0036	0.011	0.009

To close this system, one also needs an initial condition, $T(t=0,z)$, a top boundary condition, $T(t,z=0)$, and a bottom boundary condition, $T(t,z\rightarrow\infty)$. This is a second order partial differential equation with respect to time and space. The analytic solution of this heat flow model has been thoroughly studied since the 1800s [2]; its solution, given a variety of initial and boundary conditions, can be found in current literature such as [1]. For instance, if we consider the following boundary conditions:

$$T(0,t) = T_a + A\,sin(\omega\,t+\phi) \tag{3}$$

and

$$\lim_{z\rightarrow\infty} T(z,t) = T_a \tag{4}$$

an analytic solution to Eq.(1) is given by

$$T(z,t) = T_a + A\,e^{-\frac{z}{D}} sin[\omega\,t - \frac{z}{D} + \phi], D = \sqrt{\frac{2K}{\omega}}. \tag{5}$$

Eq.(3) indicates a sinusoidal temperature pattern at the top of the soil column where the sunlight directly impacts. Eq.(4) implies that when it is sufficiently deep below the surface, the soil temperature converges to the average subsurface temperature T_a and is independent of time.

For a homogeneous system, the thermal conductivity of the soil column is a constant value K throughout the domain. In our study of a heterogeneous system however, the thermal conductivity can vary by depth and is a mapping from the seven spatial intervals in Z to seven values of K: $\{K_i \mid i \in Z\}$, where $Z = \{(0\sim 1),(1\sim 5),(5\sim 10),(10\sim 15),(15\sim 20),(20\sim 25),(25\sim 30)cm\}$.

2.2 Estimating Thermal Conductivities

In this project, discrete values of the temperature at 5 min time intervals are already known while the thermal conductivities K are unknown. Figure 1 plots the given temperature data over time and space. The temperatures range from about 13 to 67 ^oC in the first 24 hours. To inversely determine the K, we took two approaches. In the first approach, thermal conductivities are calculated using analytic methods. In the second attempt, we cast this problem to an optimization frame where the least-squares error (LSE) between data and simulated temperature profile is minimized. Specifically, the logged data T^{obs} is a $N_t \times N_z$ matrix where N_t is the number of time points and N_z is the number of spatial nodes; the simulated temperature profile $\hat{T}(K)$ is obtained by numerically solving the heat equation where the boundary conditions come from data and K is a guessed

value (for homogeneous system) at each iteration of the optimization scheme. We pose this idea mathematically as:

$$\min_{K\in\Omega} J(K) = \frac{1}{2}\sum_{i=1}^{N} w_i(\hat{T}_i(K) - T_i^{obs})^2, \tag{6}$$

where Ω represents reasonable bound constraints on K, w_i are algorithmic weights. In the case of a heterogeneous system, the K in Eq.(6) will be replaced with the set of K values described in Section 2.1.

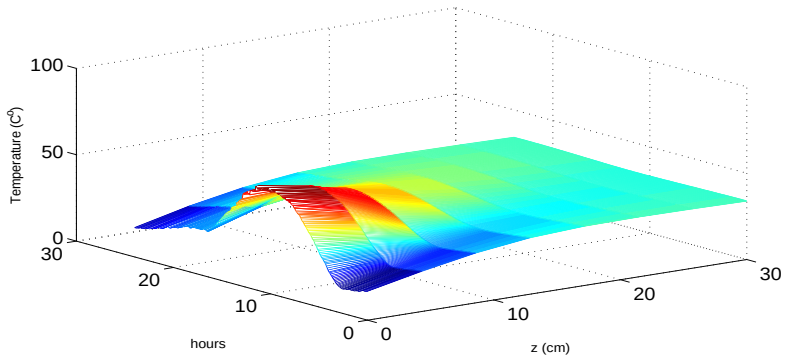

Figure 1: Temperature data

2.3 Boundary Conditions

Several additional numerical experiments were conducted to understand how boundary condition implementation could best match the data acquisition capabilities of the sensors. The top boundary condition was implemented in a straight forward way as a time dependent Dirichlet condition, $T(t, z_{top})$, using the data collected at the first sensor. Section 3.3 will discuss the details of including data as boundary condition.

2.4 Initial Conditions

The initial condition of the system is implemented using the temperature data taken at the first time step, or the first row of the data matrix. Here, $T(x, t = 0)$ is a mapping from the eight sensor locations to eight temperature values.

3 Parameter Identification Using Optimization

In this part, we consider a heterogeneous system that can be described using a slight variation of Eq.(1):

$$\frac{\partial T}{\partial t} = \frac{\partial}{\partial z}[K\frac{\partial T}{\partial z}] = K\frac{\partial^2 T}{\partial z^2} + \frac{\partial K}{\partial z}\frac{\partial T}{\partial z}, \tag{7}$$

where $K = K(z)$ is a function of spatial variable z. Finite differences were used to discretize Eq.(7) and a centered difference is used for $\frac{\partial T}{\partial z}$. The numerical solver has been validated using a test problem where a forcing term $f(z,t)$ is added to the right side and the function $K(z)$ is known. Since we only consider K values at seven locations, we use a spline over space to create a continuous function where K is specified at all locations. The derivative of the continuous spline function is then used to account for the $\frac{\partial K}{\partial z}$ term in Eq.(7).

Figure 2 shows the structure of the optimization scheme for a heterogeneous system. At each iteration, the optimizer will, based on the bounds Ω and previous function evaluations, pick a set of six K values as input for the numerical solver for the heat equation that outputs the temperature profile. The simulated profile is then compared to actual data to obtain the error at current iteration. The optimization terminates when the error becomes sufficiently small and the current set of K values is a potential optimal solution. Both the genetic algorithm ([6]) and the implicit filtering ([5]) are used as optimizers in this process.

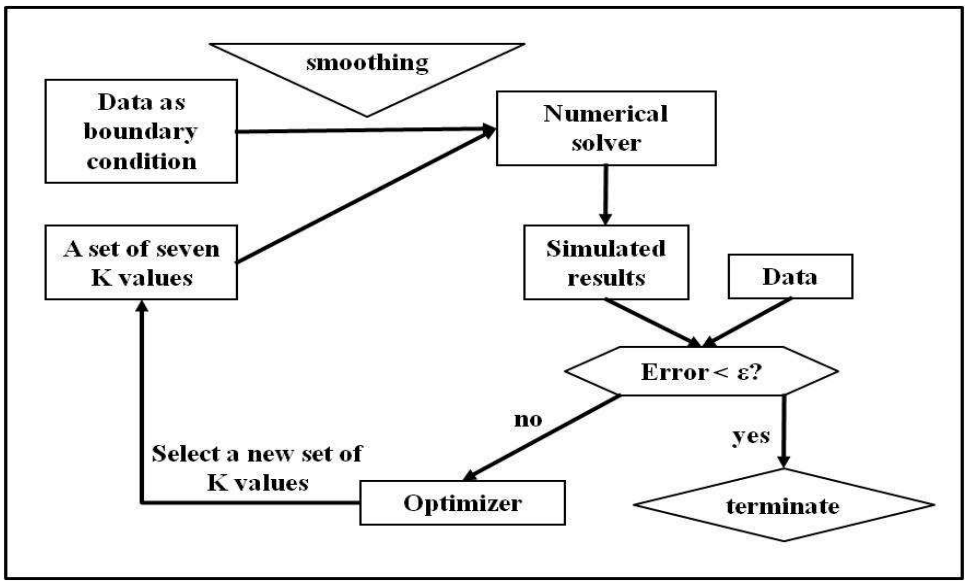

Figure 2: Structure of the Optimization Scheme

With the working simulation tool in hand, we used the genetic algorithm and the implicit filtering algorithm to fit the data profile in all layers at the 24th hour by optimizing the set of conductivities at six layers described in Sec.(2.1). In our first attempt, we assumed that the conductivity is a linear function over space in each layer. Thus, to create a continuous function $K(z)$, we simply used a linear spline curving-fitting technique. We enforced 70cm to be the bottom depth and assumed that the conductivity at layer 0-1cm and 30cm-70cm (bottom) are constant and are equal to

K_{1-5cm} and $K_{25-30cm}$ respectively. In our simulation, $\Delta z = 0.1cm$ and $\Delta t = 0.1$ minutes. Table 2 shows the optimal conductivity values obtained for each depth using genetic algorithm when the results are optimized at the 24^{th} hour data.The last two rows show the sLSE (see Eq.8 for definition of sLSE) and the maximum temperature difference (E) at the final time.

Table 2: Preliminary optimization results

Depth	K (cm/min)
1 cm	3.2809e-002
5 cm	3.1440e-001
10 cm	2.6486e-002
15 cm	3.9509e-001
20 cm	1.9201e-001
25 cm	9.8476e-003
30 cm	2.6704e-001
Temp (^oC)	35.33
sLSE	5.9633e-005
E (^oC)	0.895

3.1 Experimentation on Implementation Details

The above results inspired a series of studies in regards to the choices made in the original modeling and optimization process to understand how these choices impact the optimal solution and its simulation fittings at intermediate time points. The set of experimentations are summarized and described here:

Section 3.2: Assumptions on Conductivities

In this study, we explored how different implementations on the heterogeneity of the system influence the stability of the simulator. Specifically, we tested the simulator with K vectors that are 1) linearly connected; 2) cubic splined; 3) interpolated using a hybrid method.

Section 3.3: Low Amplitude Noise in Top Boundary Condition

Noises in data are inevitable due to uncertainties in environment. In this section, we analyzed the impact of low amplitude noises in the top boundary data on the stability of the simulator.

Section 3.4: Using 30cm as Bottom Boundary Condition

In our first attempt, the simulator used 70cm as the bottom depth and assumed a constant temperature as the bottom boundary condition. In this experiment, we leveled up the bottom depth to 30cm, where the bottom boundary condition is available from recorded data. We are interested to see if this change will improve the accuracy of the simulator since more information will be given.

Section 3.5: Time Dependent Thermal Conductivities

The physics in the subsurface environment can change over time due to conditions such

as increased water content from rainfall. Although thermal conductivities (K) are constant over time, change in physical environment can impact the conductivities of heat in the system via other parameters. To incorporate the possible time dependency, we assumed that thermal conductivities may vary on a three hour interval. We seek to examine whether this assumption may improve the estimation accuracy.

Section 3.6: Top Surface Data Elimination

The micro environment can change constantly around the top surface censor due to human activities and natural impacts such as rainfalls. Such change can introduce bad noises into the data at 0cm and 1cm. In this study, we avoided using data at 0cm and 1cm and only optimize from 5cm to 30cm. This effort is made to look for further improvement in the stability of the simulator.

Section 3.7: Guided optimization: Error calculation over all time points

In our first attempt, the optimizer only minimizes the error at the final time of simulation. However, the objective this work is to determine a set of thermal conductivities that simulates temperature profiles that fit the data throughout the time domain. In this study, we re-designed the error calculation formula so that it incorporates fitting error at other times as well.

The purpose of these studies is to tailor the simulator and optimization framework to its best ability to make accurate estimations on the thermal conductivities. The following sections are dedicated to these studies and their results.

3.2 Assumptions on Conductivities

Initially, to model the heterogenity of the system, seven conductivity values are connected using linear functions and thus the derivative is piece-wise constant. Although several optimization runs produced reasonable LSE, the solution showed sensitivity to sharp changes in conductivity values. To smooth out the sharp transitions in K, we replaced the linear interpolation with cubic spline. However, since there are only seven values over a domain of 30cm, cubic spline over the sparse data resulted in concavity in the curve that produced unrealistic negative K values. Finally, we implemented a moving average method to smooth out the curve while avoiding unwanted concavity. This is done by the following three steps:

1. apply linear spline to the seven K values to obtain a denser value set;
2. use moving average to filter out the noises in the denser set and obtain a smooth set;
3. apply cubic spline to the smoothed value set.

Step 1 inserts values among the original seven points to help guide the construction of cubic spline in Step 3; this way, unwanted concavity can be avoided. The reason to use cubic spline in the last step is to obtain the polynomial coefficients to differentiate the spline function for the $\frac{\partial K}{\partial z}$ term in Eq.(7), which are now quadratic and are smooth at the spline knots (the sensor locations). Figure 3 shows a comparison among the different methods of handling the K values. Here, we used

a generic K vector for demonstration purpose. As seen from the graph, the hybrid moving average method agree at most locations with the linear spline but have softer transitions; meanwhile, the moving average does not create negative K values as the cubic spline does. The stability of the simulation tool was improved after the implementation of the moving spline method and thereby the simulation results are improved.

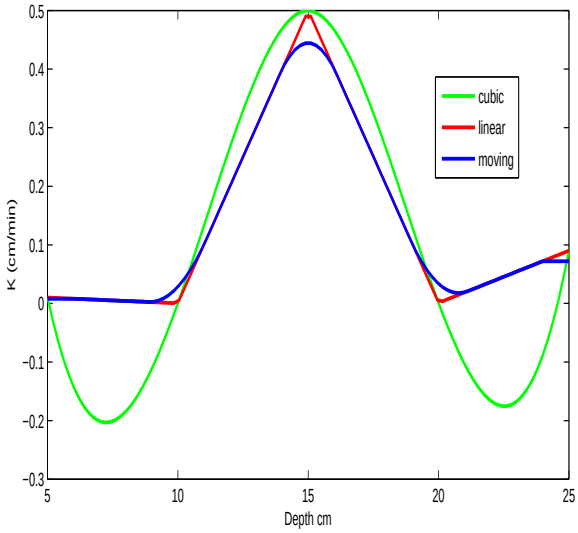

Figure 3: Comparison of methods for incorporating thermal conductivities

3.3 Low Amplitude Noise in Top Boundary Condition

The top boundary condition used in the numerical solver comes from data at 0cm over the first 24 hours. Figure 4 is a graphical interpretation of the data. Notice that there are large temperature oscillations of about $3 - 5^oC$ over a sufficiently small time interval in the middle of the curve. We suspect that this low amplitude noise may impact the fit at 1cm point. Furthermore, initial simulation experiments showed sensitivities to the values of K at the 1cm point; in other words, small changes in the conductivity at 1cm lead to large changes in the LSE. This observation is part of the motivation of omitting data at 1cm and instead using a six layer system described in Sec. 2.1 for the study below. In this part, we used a convolution to filter out the low amplitude noise in the top boundary condition. Figure 5 shows the resulting top boundary profile. However, no significant improvement in LSE was found in this study.

3.4 Using 30cm as Bottom Boundary Condition

The purpose of this study is to remove the influence of the missing bottom boundary condition and initial data on the optimization as mentioned in the end of Sec.3. Here we consider a five layer system where we only identify the conductivity values at 5 ($1 \sim 5$),10 ($5 \sim 10$),15 ($10 \sim 15$),20 ($15 \sim 20$) and 25 ($20 \sim 25$) cm layer. The bottom depth is set at 30cm (instead of 70cm) and a spline of the data at 30cm is used as the bottom boundary condition. We also run optimization

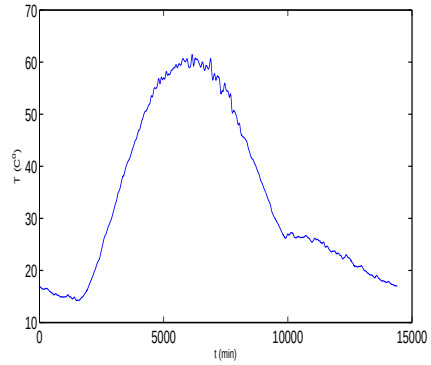

Figure 4: Top boundary condition

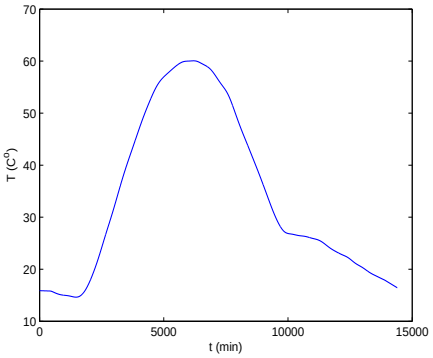

Figure 5: Filtered top boundary condition

experiments to fit the final temperature data profile at 6,12,18 and 24th hour to observe the variation in the optimal conductivity sets. The data profiles at 6, 12, 18 and 24th hour is plotted in Figure 6.

Table 3 shows the optimal set of K values when fitting at four different final times. Notice that the LSE is significantly larger by an order of two in the 18th and 24th hour trial. Multiple optimization runs using different optimizers were carried out in an attempt to improve the results for the 18th and 24th hour experiments but little improvement was seen.

Table 3: Best-fit K values at 6, 12, 18, and 24 hours using 30cm as the bottom boundary condition

Final Time	K_5	K_{10}	K_{15}	K_{20}	K_{25}	LSE
6hr	0.0821	0.4872	0.3459	0.4998	0.4998	5.4358e-001
12hr	0.1314	0.2592	0.1682	0.3842	0.2822	2.8560e-002
18 hr	0.0924	0.5000	0.00001	0.5000	0.375	3.5162
24 hr	0.007	0.0004	0.4999	1.3431e-05	0.5000	7.41

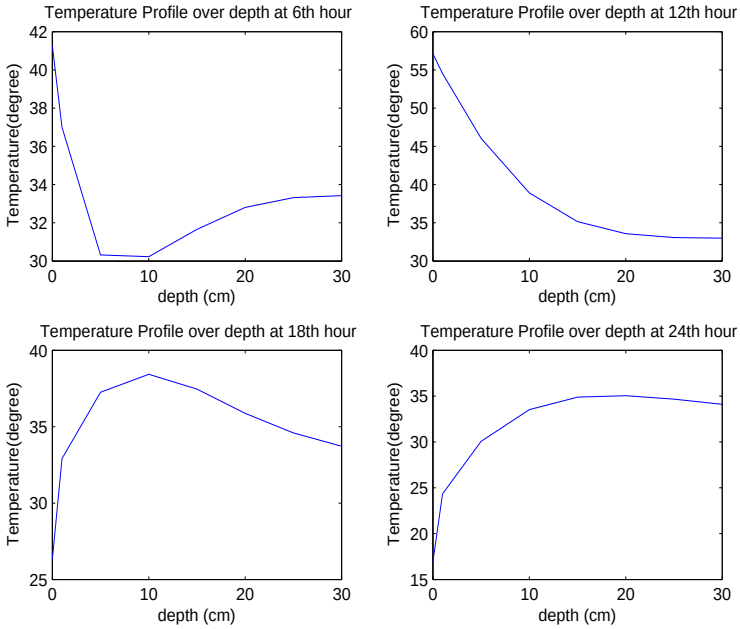

Figure 6: Temperature profiles at 6, 12, 18, and 24 hours

3.5 Time dependent conductivities

To this end, we have come to the conclusion that certain aspects of this problem is causing instability issues in our simulation and optimization. Specifically, we observed difficulties in optimization with data over longer time intervals, e.g. 18 and 24 hours, is more challenging as shown in Table 3 with the larger LSE.The physics in the subsurface environment can change over time due to conditions such as increased water content from rainfall. Although thermal conductivities (K) are constant over time, change in physical environment can impact the conductivities of heat in the system via other parameters. In other words, the combined value of K and other parameter such as moisture content may change during longer time frame. With this thought, we conducted another set of experiments where the optimization was processed over a three hour interval data, assuming that the K values are constant within a three hour span. The results are shown in Table 4.

Table 4: K values when optimize over 3 hour intervals

Interval	K_1	K_5	K_{10}	K_{15}	K_{20}	K_{25}	LSE
0-3 hr	**0.0313**	0.3180	0.0465	0.3798	0.0088	0.8812	0.07
3-6 hr	0.1502	0.3502	0.0254	0.7311	0.0099	0.9937	0.02
6-9 hr	0.0887	0.2413	0.1484	0.4827	**0.0061**	0.2952	0.03
9-12 hr	**0.1168**	**0.1478**	**0.2098**	0.2261	**0.4287**	**2.1246**	0.29
12-15 hr	0.0228	**0.7370**	**0.0026**	0.7605	0.0114	0.8254	0.06
15-18 hr	0.0323	0.4304	0.2757	0.1913	0.2696	0.3742	0.05
18-21 hr	0.0351	0.4257	0.0826	0.0157	0.3123	**0.1402**	0.13
21-24 hr	0.0328	0.3937	0.0487	0.5782	0.1535	0.2391	0.13

The new assumption has improved the results by a noticable amount. The maximum LSE among all trials is 0.29 and the rest majority is around 1E-2, which is a significant reduction over the LSE of 7.41 from the previous 24 hour simulation. However, unexplained instability remained in the K values. For example, as shown in Table 4, the K value at 20cm jumped from 0.0061 to 0.4287 over a course of 3 hours. Other noticable jumps are shown in bold. Such large magnitude oscillation in K values is not usual in reality, indicating the ill-conditioning still exists in our problem structure.

Through other experiments, we also observed that 1) most optimization trials struggle with fitting the simulation at 0cm and 1cm; 2) the solution might not be unique, meaning that more than one set of K values can produce reasonable fitting.

3.6 Bad Data Elimination and Scaled Error Calculation

Top surface censors are exposed to constantly changing environment; thus the data recorded in those locations are susceptible bad noises. Such noise could severely corrupt the simulation by introducing unwanted trends into the system. In this study, we avoid using the data at 0cm and 1cm and only consider data from 5-30cm. To accommodate for this change, the K values at 0cm and 1cm are eliminated from the K vector; only K values at 5, 10, 15, 20, 25, and 30cm are being searched for. In addition, the top boundary condition changed to the data measured at 5cm instead of at 0cm.

Furthermore, a scaled LSE calculation is used for the following set of experiemnts for better cross-trial comparison. We denote the scaled LSE with **sLSE**, which is calculated as:

$$sLSE = \frac{1}{2}\frac{\sum_{i=1}^{N} w_i(\hat{T}_i(K) - T_i^{obs})^2}{\sum_{i=1}^{N}(T_i^{obs})^2}, N_t = 1 \tag{8}$$

, where N_t is the number of time points and is set to 1, which is the final time node. Here, the normal LSE is scaled by the summation of squared data values.

With the updated simulator, same experiments as decribed in Section 3.4(results shown in Table 3) are conducted. Table 5 shows the new results:

Table 5: Best-fit K values at 6, 12, 18, and 24 hours using the updated simulator

Final Time (trial)	K_5	K_{10}	K_{15}	K_{20}	K_{25}	K_{30}	**sLSE**
6hr	0.2308	0.1415	0.3300	0.2662	1.3652	2.0000	3.3559e-007
12hr	0.1722	0.2041	0.2253	0.3968	0.0553	0.0625	1.2309e-006
18 hr	0.2990	0.2335	0.2171	0.3553	0.4738	0.6681	8.1094e-008
24 hr	0.1563	0.1538	0.1646	0.3704	0.1582	0.3372	2.4496e-007

Notice that the scale of *sLSE* is obviously smaller than *LSE* due to the scaling; it is not wise to compare the errors in Table 3 to the errors in Table 5.

The stability of the new results have significantly improved as shown in the table. The sLSE for all four trials are on a similar scale and are reasonably small. On the other hand, however, the optimal set of K values vary by a noticable amount at 25cm and 30cm over time. Such oscillation is not expected and indicates instability in the simulator. An alternative approach to analyze the

quality of a K set estimation is to examine the fittings of its simulation at other times other than the final time of optimization. For instance, Figure 7 and Table 6 show the fittings at 6, 12, 18, and 24 hours using the K values from the third trial (18 hour as final time).

Figure 7 and Table 6 have both indicated that the fitting at 18 hour is signigicantly better than fittings at other hours. Using the K values from the 18 hour trial to predict the profile at a future time, 24th hour, is particularly challenging as indicated by the large sLSE. Since the optimization in the 18 hour trial is guided towards minizing the error at that hour, the observed biased behaviour is reasonable; however such temporal bias should be eliminated since we are trying to fit the profile at all times.

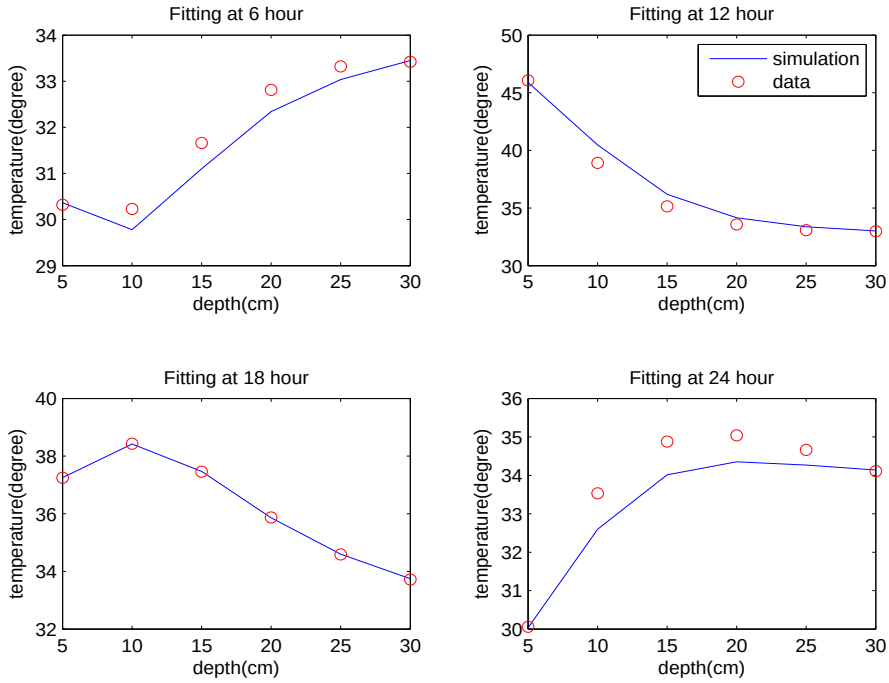

Figure 7: Profile fittings at different times using optimal K values from the 18 hour trial

Table 6: sLSE of fittings at different times using optimal K values from the 18 hour trial

Fitting at	6 hour	12 hour	18 hour	24 hour
sLSE	6.6541e-005	2.4030e-004	8.0971e-008	1.6450e-004

3.7 Guided optimization: Error calculation over all time points

To resolve the biased optimization described in the previous section, we revised the error calculation so that it evaluates the fittings at all discrete time nodes:

$$nLSE = \frac{1}{2}\frac{\sum_{i=1}^{N} w_i(\hat{T}_i(K) - T_i^{obs})^2}{\sum_{i=1}^{N}(T_i^{obs})^2}, N_t = 289 \tag{9}$$

, N_t is the number of time points. The number of time steps in the current simulator is 14400 over a span of 24 hours; however, to save data storage, we set $N_t = 289$ to match the first 24 hour data, which has 289 time nodes (measure every five minutes); this is done by saving the simulation result at every 50th time step. With the new error calculation, denoted as **nLSE**, the optimizer is guided to find a solution that fits the temperature profile at all times, other than just at the final time.

Table 7 shows the updated results of the same experiments as conducted in Section 3.4 and Section 3.6(results shown in Table 3 and Table 5 respectively). In the updated results, the oscillation of solutions among different trials have significantly decreased; the difference between solutions from the 18 hour trial and 24 hour trial can be considered trivial. Furthermore, the nLSE decreases monotonically as the final time increases.

Table 7: Using nLSE calculation, results when optimize to different final time

Final time	K_5	K_{10}	K_{15}	K_{20}	K_{25}	K_{30}	**nLSE**
6 hour	0.1000	0.2250	0.1000	0.2875	0.2250	0.2875	1.1634e-005
12 hour	0.1669	0.1533	0.1916	0.3008	0.3079	0.5992	7.5479e-006
18 hour	0.1718	0.1637	0.2178	0.2169	0.3267	0.2651	5.3053e-006
24 hour	0.1724	0.1579	0.2151	0.1988	0.2783	0.2242	4.0694e-006

To examine how well each solutions from Table 7 fit the profiles at other times, we ran simulations over 24 hours using each of the four sets of K values from the table and compared the profiles at 6, 12, 18 and 24 hour. Table 8 presents the results. For example, the entry in row 2 and column 5 is the sLSE of the solution at the 24th hour when simulated using the K values from the 12 hour final time trial. For each trial (row), the sLSE in bold is the smallest among all errors in that row. Notice that the minimum sLSE does not necessarily occur at the same time as the final time of the optimization. For instance, the smallest sLSE for the 6 hour final time trial occurred at the 24th hour. This is a strong argument for an unbiased optimization.

Table 8: Fitting errors (sLSE) comparison when using optimal Ks from different trials

Trial	$sLSE_6$	$sLSE_{12}$	$sLSE_{18}$	$sLSE_{24}$
$K6$	1.2249e-005	2.2495e-005	2.5854e-005	**6.8053e-006**
$K12$	**2.8981e-006**	5.5453e-006	2.1316e-005	2.0589e-005
$K18$	5.3504e-006	1.4656e-006	**8.4758e-007**	3.4899e-006
$K24$	4.1154e-006	2.6162e-006	7.3536e-007	**9.5003e-008**

Since the 24 hour trial has the smallest nLSE overall, we selected its corresponding optimal K values to examine the fittings at other times graphically. Figure 8 shows the fitting at all four hours; the fittings are greatly improved compared to Figure 7. Through numerical calculation, the

maximum error in this trial is found to be 1.1 ^oC, which is within the range of machine error as provided by the collaborator. This value is also significantly smaller than 6.2 ^oC as recorded in Table 2 using the older version of the simulator.

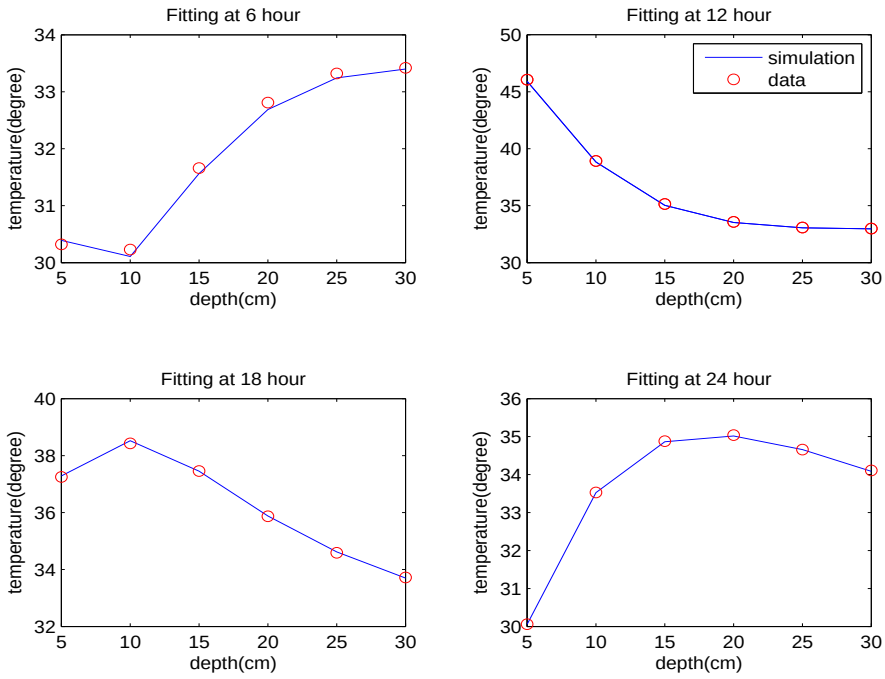

Figure 8: Under unbiased optimization: profile fittings at different times using optimal K values from the 24 hour trial

3.8 Summary of Implementation Experiments

To this end, we have completed a series experiments that help us with the choices made to tailor the simulator and optimization set up to its best functionality. To summarize the features in the final setup of our simulator:

- Top Boundary Condition: data at 5cm
- Bottom Boundary Condition: data at 30cm
- K values interpolated using hybrid method
- Objective function: Error calculated using Eq.9

With the current setup, we are able to predict a set of K values that simulates reasonably fitting temperature profiles at all times.

As will be discussed in the next two sections, measurement errors from the sensor are introduced to the simulator through the boundary and initial conditions; such error can not be eliminated

using numerical scheme, however it will dissipate out of the system over time. In the fifth row of Table 8, the sLSE decreases monotonically over time and the error at 24th hour can be seen as insignificant. This dissipation behavior validates the analytical study of error propagation and sensitivity analysis of the simulator discussed in Section 4 and Section 5.

4 Sensitivity Study On Homogeneous Model

The study above identifies a potential set of thermal conductivities for the specific site where the temperature data is taken. However, errors in this estimation process can be introduced in two ways: 1) errors in temperature measurement, and 2) system errors from numerical methods. These two types of errors combined decide the accuracy of our estimation. System error is often inevitable and hard to predict due to the nature of numerical estimation; however, errors from data can be determined via specifications of the measuring infrastructure (e.g the temperature sensor used in the study). A sensitivity study is where we analyze how the known error from initial setup of the system impacts the final results. It provides guidance on how much one should trust the estimation.

In this section, we present a series of numerical experiments to gain insight to the error propagation pattern in heat equation. Specifically, we study the impact of various types of errors in the initial condition (data) and the speed with which they dissipate in the final solution for a *homogeneous system*. We also analyze the spatial pattern of error propagation; that is, at what point in space (depth, in this case), the error becomes insignificant.

We consider Eq.(5) with a simplified case where $A = 1$, $T_a = 0$, $\omega = 1$, $\phi = 0$, and $K = 1$. The resulting analytical solution is:

$$T(z,t) = e^{-z/\sqrt{2}} sin(t - z/\sqrt{2}). \tag{10}$$

Setting $t = 0$ in Eq.(10), we obtained the initial condition for the simplified case:

$$T(z,0) = e^{-z/\sqrt{2}} sin(-z/\sqrt{2}) \tag{11}$$

Since the motivation for this work involves incorporating data into a simulation tool for heat transport, we solve Eq.(1) numerically and compare our results to the true solution given by Eq.(10) to understand how variations of initial condition (Eq.(11)) impact the computed solution. We use backward Euler in time with finite-differences in space, resulting in an approach that is first order in time and second order in space. Table 9 shows the spatial and temporal parameters. Thus, our numerical error will be $\mathcal{O}(10^{-4})$. A grid refinement study was done to ensure the simulation tool obtained the correct accuracy prior to these experiments.

Table 9: Finite difference parameters used in numerical simulator

Domain size (cm)	Spatial step (cm)	Duration of simulation (min.)	Time step (min)
30	Δz =0.025	1000	Δt = 6.25e-04

4.1 Type I Error

In this experiment, we introduce an error in the initial condition described in Eq(11) with an additive term ϵ to get

$$T(z,0) = e^{-z/\sqrt{2}} sin(t/\sqrt{2}) + \epsilon. \tag{12}$$

4.1.1 Numerical Experiments

From Eq (11), the range of the true initial condition is between -0.3 to +0.1 C^o; therefore, we set ϵ to approximately $\pm 10\%$,$\pm 20\%$, -25% and -30% of the true value. In other words, we ran a set of simulations with error $\epsilon = \pm 0.03, \pm 0.06, -0.08, -0.1C^o$. Figure 4.1.1 shows the initial conditions with different ϵ and the true initial condition.

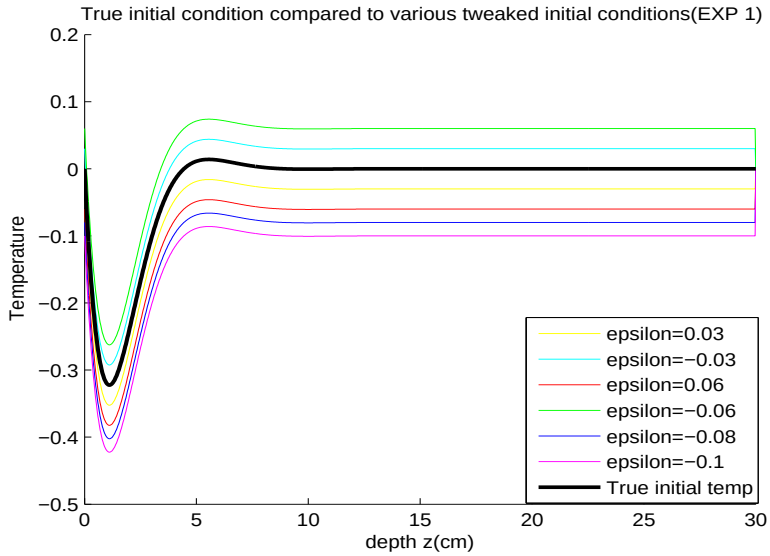

Figure 9: True initial condition compared to tweaked initial condition (Experiment I)

Errors between the simulated results and analytical solution over the entire physical domain are calculated using the infinity norm at each time step. Figure 10 shows the progression of total error over time. The error decreases over time and eventually converges to truncation error. To further illustrate how the simulated solution eventually approaches the true solution over time, we plotted the simulated solution compared to true solution at four different times in Figure 11. As can be seen from this picture, by the 398th minute (4th plot) the two curves are in close agreement.

Figure 12 shows the inifinity-norm error among all times at each grid point to help illustrate the error propogation in space. Notice that the error becomes insignificant at both the top and bottom boundary of the domain due to the Dirichlet boundary conditions. One of the interesting findings from Figure 12 is the symmetry of spatial error propagation about the 15 centimeters in depth. Further numerical experiments were conducted where the location of the bottom boundary condition was changed as far deep as to 100 cm and this trend continued.

The error propagation pattern in time and space combined was also investigated. Figure 13 shows the position in space where the maximum error occurs over time. As can be seen from this figure, the maximum error, about 10^{-2}, occurs at the top surface when simulation just started; between 1 and 550 minutes, the maximum error, between 10^{-2} and 10^{-4}, always occurs at around 15 centimeters. After the 600 minutes, the maximum error appears at the 2cm shallow surface; the magnitude of this error is 10^{-4}. In conclusion, the maximum error moves downward in space and stay around 15cm as time progresses; after about 600 minutes, the error becomes insignificant.

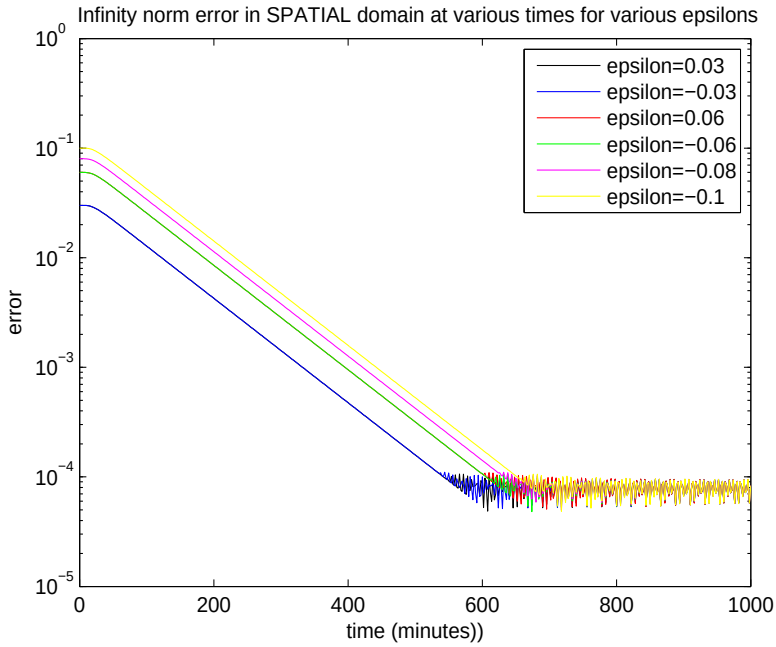

Figure 10: Infinity norm error over time (Experiment I)

4.1.2 Analysis and Error Function for Type I Error

As seen in Figure 10, the error plots of $\epsilon = -0.1, -0.08, -0.06$ and $\epsilon = 0.1, 0.08, 0.06$ overlap respectively. This implies that the trend of error propagation is insensitive to the sign of the error, thus we assume that:

$$E_\epsilon(t) = E_{-\epsilon}(t) \tag{13}$$

As discussed in the previous section, the rate of decrease of log error is constant in respect to different ϵ values as indicated by the linear and parallel portion of the curves in Figure 10. Thus, the error function,$E_\epsilon(t)$, has the same negative slope for all ϵ. Using linear fit technique, we calculated the rate of decreasing as:

$$\frac{dlog(E_\epsilon)}{dt} \approx -0.0048 \tag{14}$$

The units of this rate is $\frac{log(Error)}{time}$, since the linearity is shown in the log plot of error.

Next, we construct the line that describes the log of the error over time for different ϵ. Figure 10 shows that the log error stays constant until the time reaches about 20 minutes. Further data analysis confirmed that this occurs at 24th minute for all ϵ tested in Experiment I. This implies that the linear error equation for each ϵ always passes through the point $(24, log(|\epsilon|))$. Now, we can formalize our analysis with

$$log(E_\epsilon(t)) = -0.0048 \times (t - 24) + log(|\epsilon|), \tag{15}$$

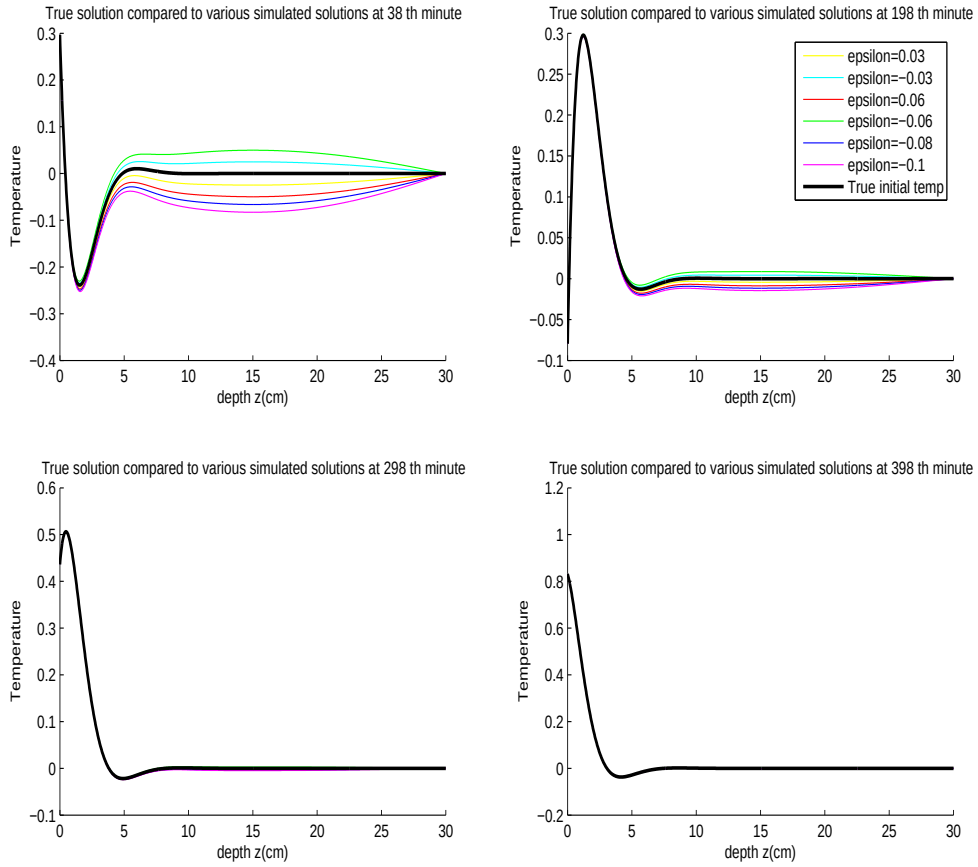

Figure 11: True solution compared to simulated solutions at various time for each ϵ, Experiment I

where

$$\begin{aligned} E_\epsilon(t) &= 10^{-0.0048\times(t-24)+log(|\epsilon|)} \\ &= |\epsilon| \times 10^{-0.0048\times(t-24)}. \end{aligned} \tag{16}$$

Figure 14 shows the original curve of $log(Error)$ over time for $\epsilon = -0.1$ and $\epsilon = -0.08$ in solid line; then the same curves are generated using equation 15 with the two different epsilons. As indicated by the graph, the fitting is accurate after the 24th minute and before the log error hits the constant of around -4, which yields the inf-norm error of around $1e-04$. Figure 15 shows the plots of the original $Error$ over time for both epsilons and then the same curves are plotted again using equation 16. Good fitting is shown in this graph as well.

Now, to validate our error model, we use Eq (16) to predict the time at which the error drops below $1e-4$ for the simulation with seeded error $\epsilon = -0.06$. We are solving for time t such that

$$E_{-0.06}(t) = |-0.06| \times 10^{-0.0048\times(t-24)} = 1e-4 \tag{17}$$

This yields a solution of $t \approx 605$, which matches what is shown in Figure 16.

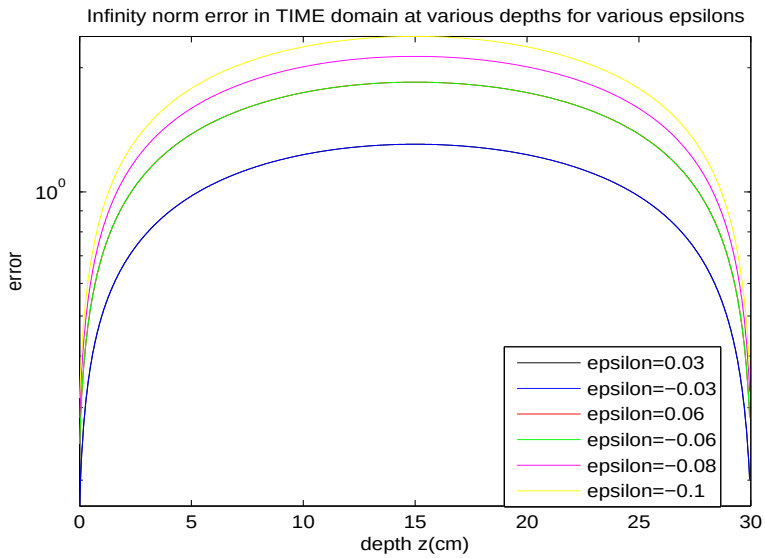

Figure 12: Total error over space from Experiment I

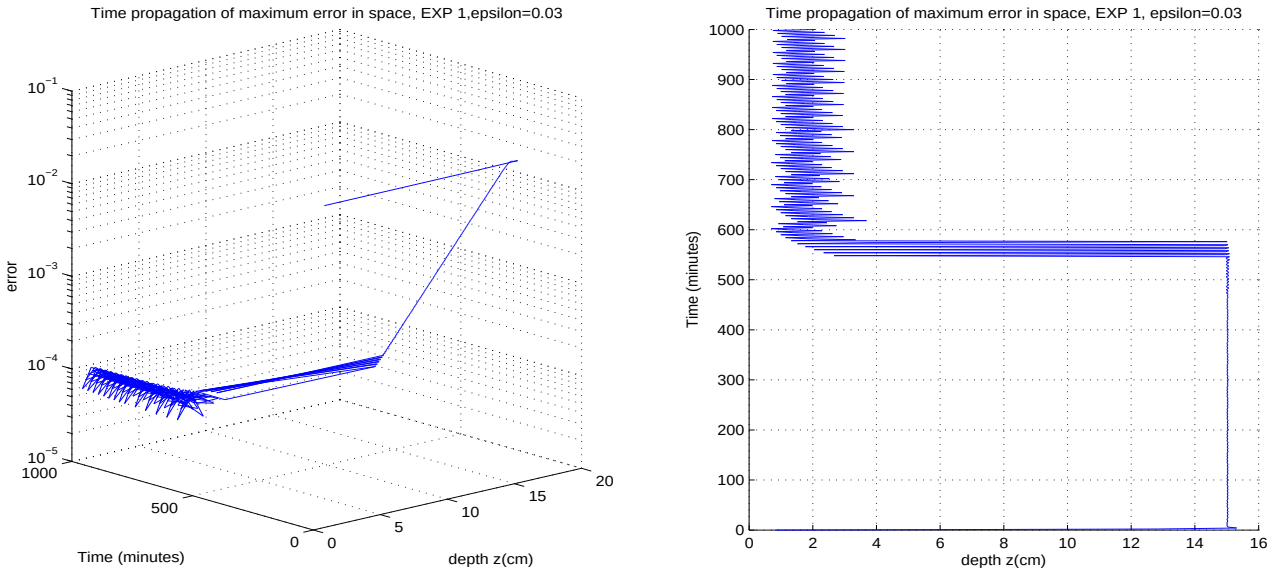

Figure 13: position of maximum error over time (Experiment I), $\epsilon = 0.03$

4.2 Type II error

In this experiment, the initial temperature is set to a constant:

$$T(z, 0) = T_0 \tag{18}$$

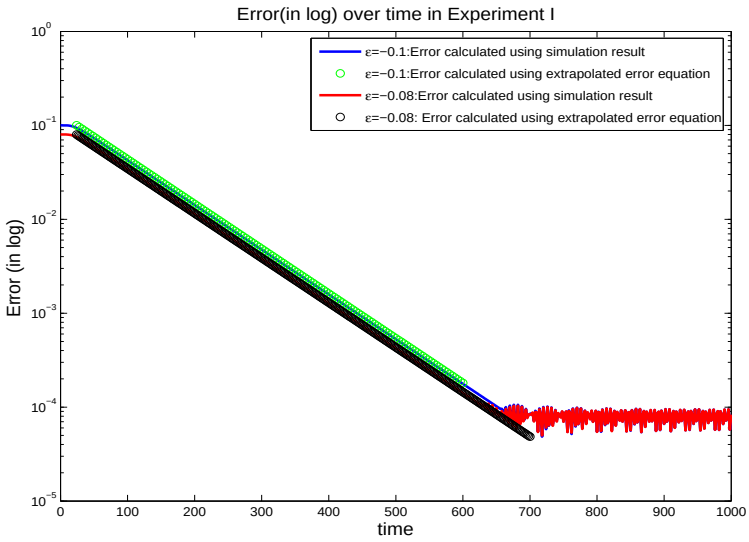

Figure 14: Experiment I: log(error) over time

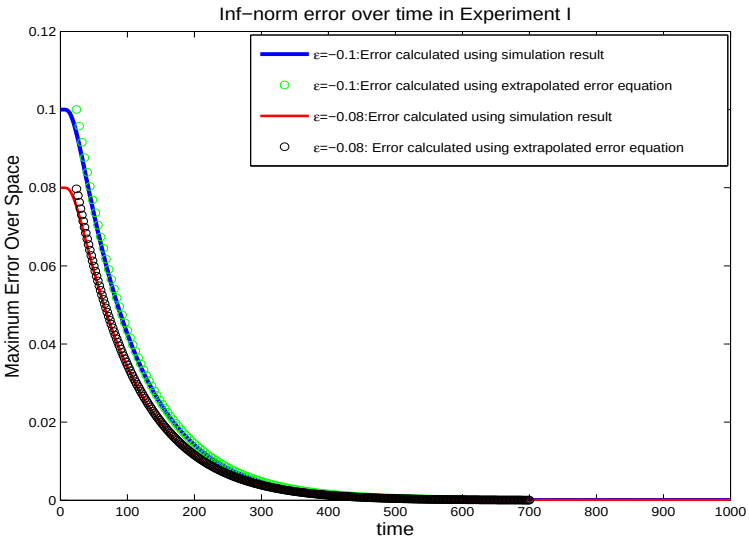

Figure 15: Experiment I: maximum error over time

4.2.1 Numerical Experiments

As mentioned in Section 4.1, the true initial condition has the range -0.3 to +0.1 C^o. Thus, to ensure that the error is not exaggerated in initial condition, we picked a set of T_0 that are close to the range: $T_0 = -0.5, -0.2, 0, 0.1, 0.4\, C^o$. Figure 17 shows the initial conditions with different T_0 versus the true initial condition.

Similar to Experiment I, we consider the pattern with which error dissipates over time and space. Figure 18 illustrates the change of infinity-norm error in space domain over time which has a similar pattern as in Experiment I. Independent of the value of the wrong initial condition, the

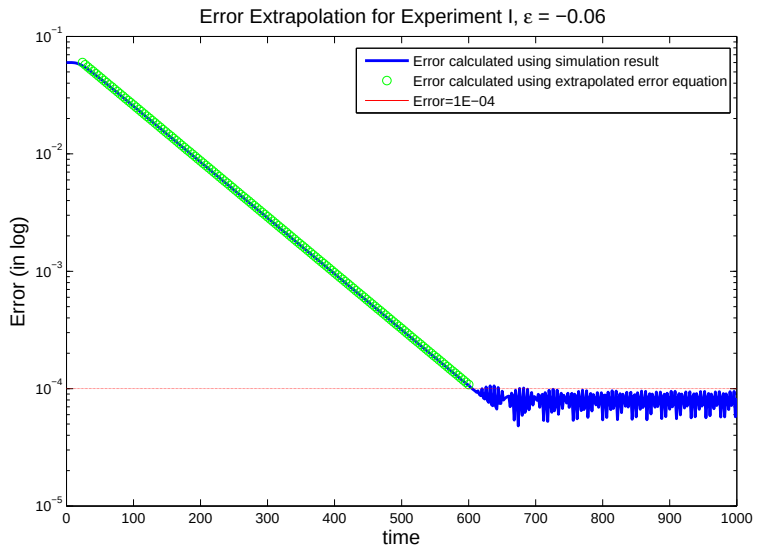

Figure 16: Model validation for Experiment I

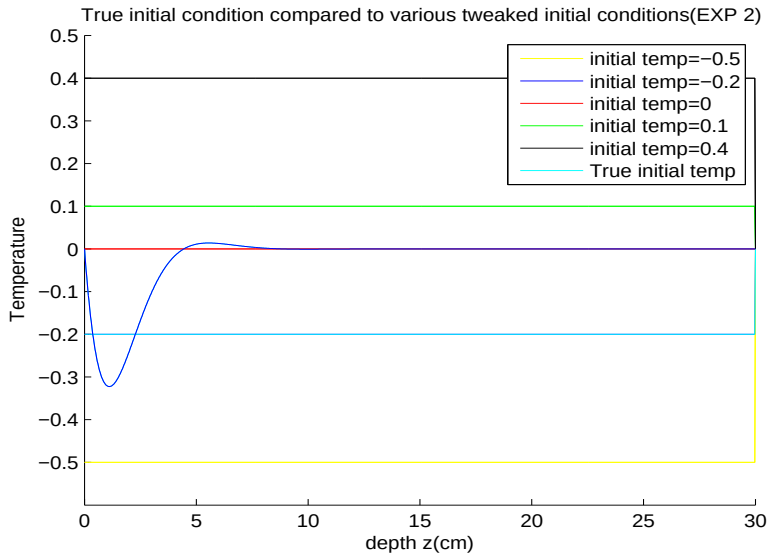

Figure 17: True initial condition compared to tweaked initial condition, Experiment II

errors all level out at the truncation error. More importantly, when $T_0 = 0$, the error decreases significantly faster compared to other wrong initial conditions. Figure 19 shows the simulated solutions versus true solution at four progressive time steps.

Figure 20 shows the infinity norm error in time domain over space which has similar spatial patterns as mentioned in Experiment I. However, when $T_0 = 0$, the symmetric space pattern about 15cm has disappeared.

In our investigation of error propagation over time and space combined, we selected the trial when $T_0 = 0$ because it appears to be different from other trials. From Figure 21, we see that the maximum error in space occurs at 1cm and works its way down to 15cm over the course of the

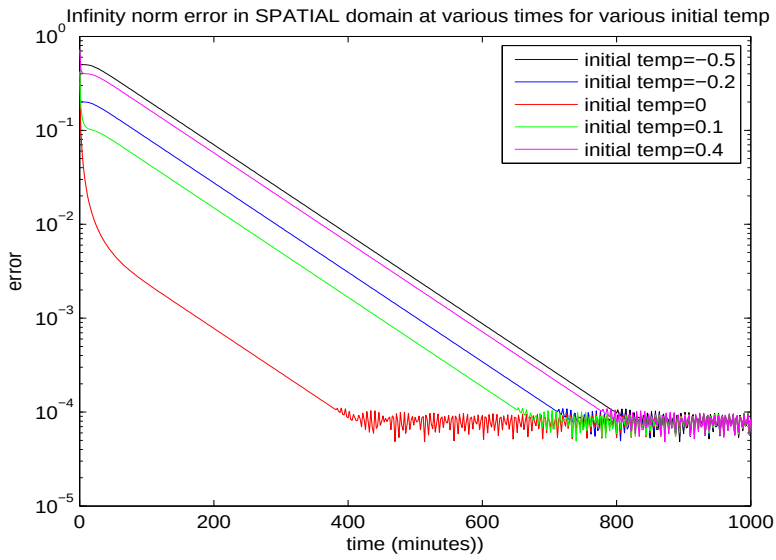

Figure 18: Inf-norm error over time from Experiment II

first 200 minutes. Then, the maximum error stays at 15cm till the 400th minute when the error becomes insignificant.

4.2.2 Analysis and Error Function for Type II Error

Previous results of error analysis for Experiment II are shown in Figure 18. Similar trends are seen compared to Experiment I:

1. the log of maximum error decreases linearly
2. the error function E_{T_0} is insensitive to the sign of the initial constant temperature T_0
3. the rate of decreasing of log error is constant in respect to T_0.

Using the same linear fitting technique, we calculate the rate of decreasing for log error over time as

$$\frac{dE_{T_0}}{dt} \approx -0.0048. \tag{19}$$

The unit of this rate is $\frac{log(Error)}{time}$. Notice that most curves shown in Figure 18 pass through points $(24, log(T_0))$ except for when $T_0 = 0$. The exception at $T_0 = 0$ can be justified since $log(0) \to \infty$. Therefor, in this error function, we omit the case when $T_0 = 0$. The model is then given by

$$log(E_{T_0}(t)) = -0.0048 \times (t - 24) + log(|T_0|), \tag{20}$$

where

$$\begin{aligned} E_{T_0}(t) &= 10^{-0.0048\times(t-24)+log(|T_0|)} \\ &= |T_0| \times 10^{-0.0048\times(t-24)}. \end{aligned} \tag{21}$$

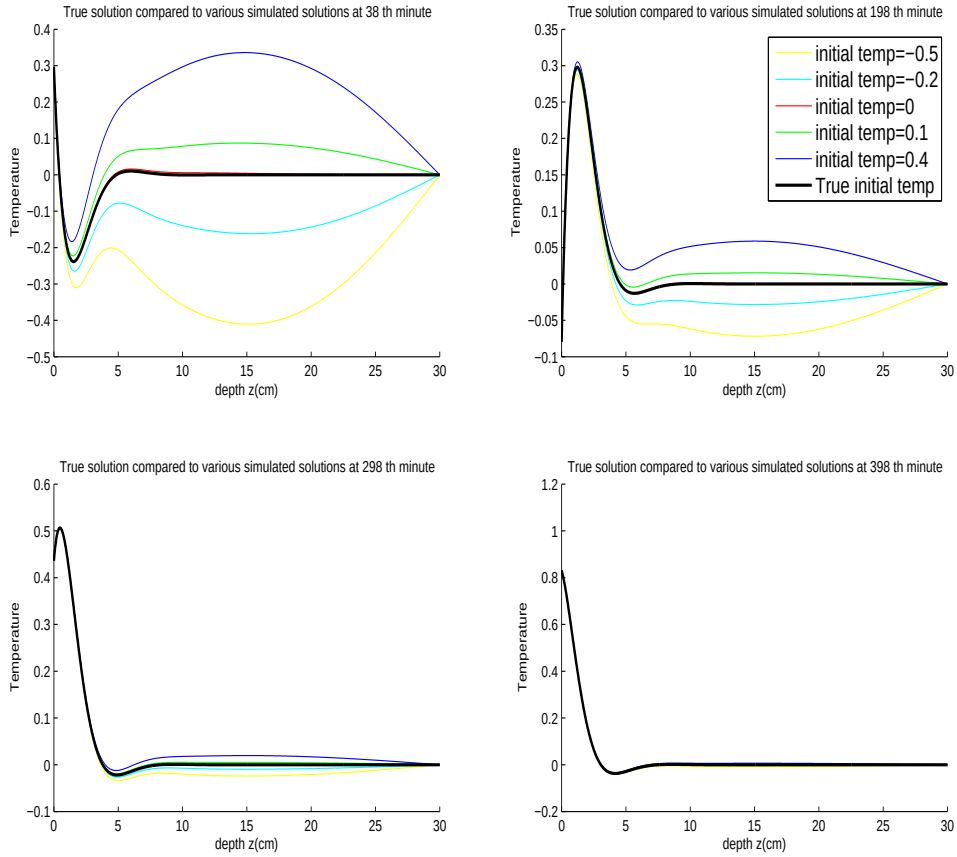

Figure 19: True solution compared to simulated solutions at various time for each T_0, Experiment II

Notice that, even though the magnitude of initial error for Experiment II is $1e-01$ while the magnitude of initial error for Experiment I is around $1e-02$, both of the error equations have the same coefficients and constants. In other words, the error equation is independent of the types of errors considered here.

To justify our fitting results, Figure 22 shows the original curve of $log(Error)$ over time for $T_0 = 0$ and $T_0 = -0.2$ in solid line; then the same plots are generated using Eq (20) with the two different T_0. Figure 23 shows the plots of the original $Error$ over time for both T_0 and then the same curves are plotted again using Eq (21). We validate the second error function model using the same approach in Experiment I. By solving Eq (22), we are able to predict that at $t = 798$, the error reaches around $1e-4$. This prediction is verified in figure 24

$$E_{T_0=0.5}(t) = |0.5| \times 10^{-0.0048\times(t-24)} = 1e-4 \tag{22}$$

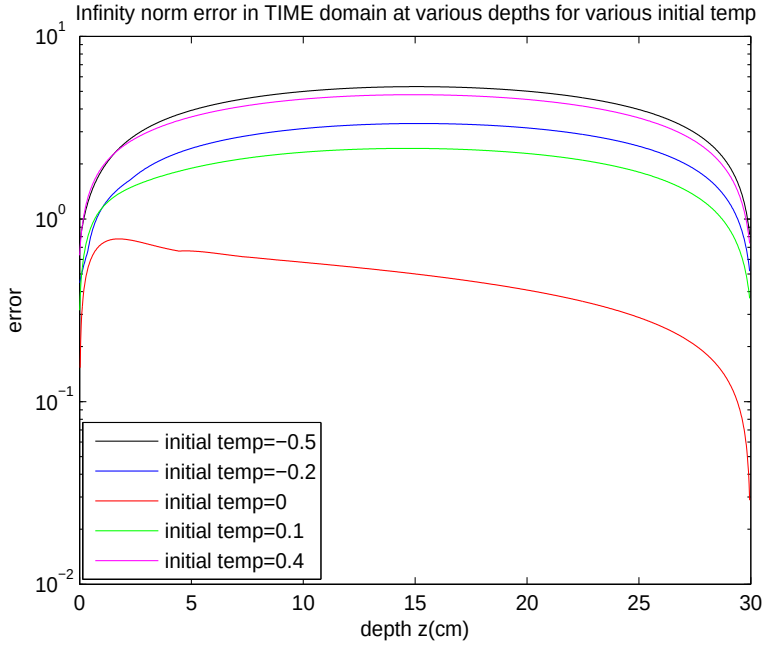

Figure 20: Total error over space from Experiment II

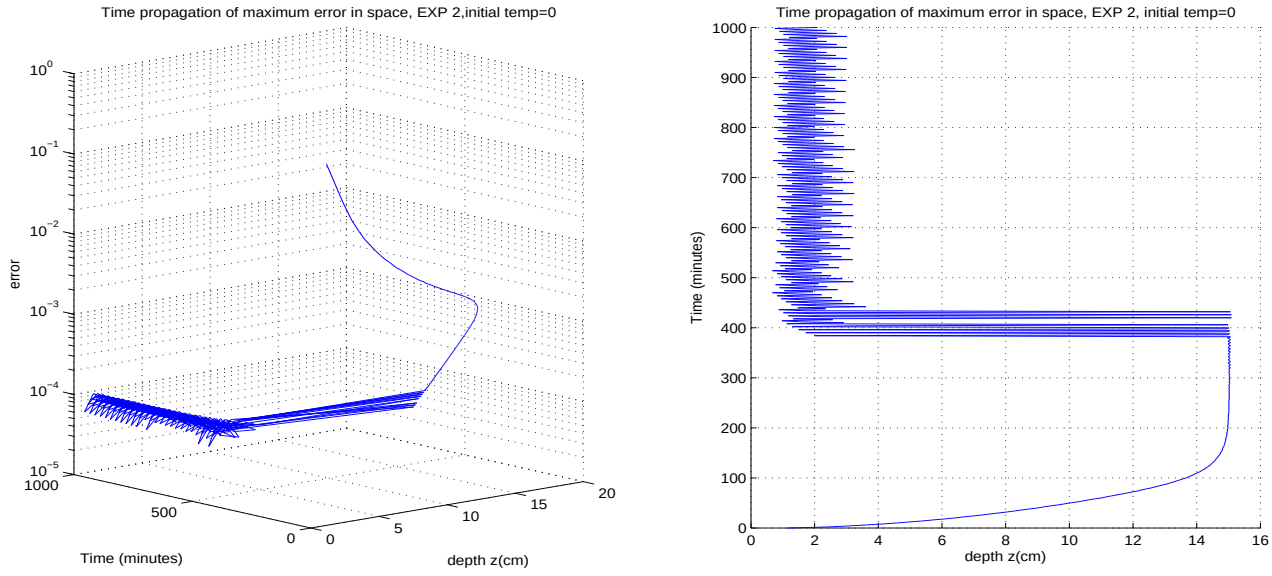

Figure 21: position of maximum error over time, from Experiment II, $T_0 = 0$

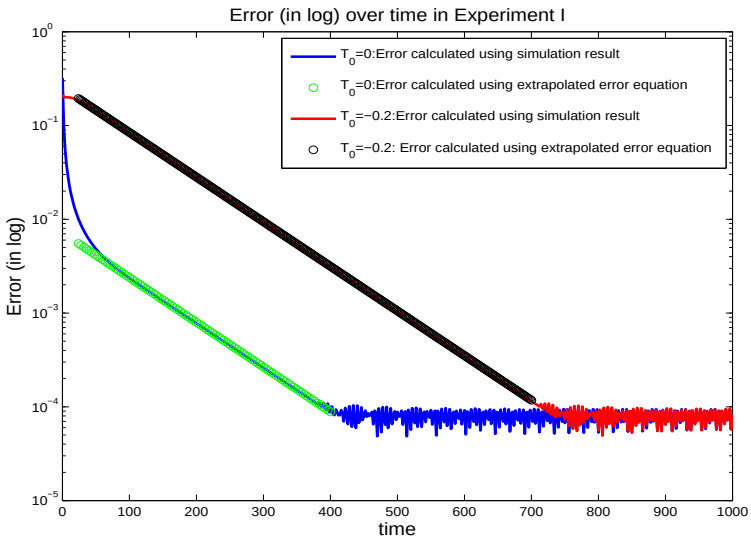

Figure 22: Experiment II: log(error) over time

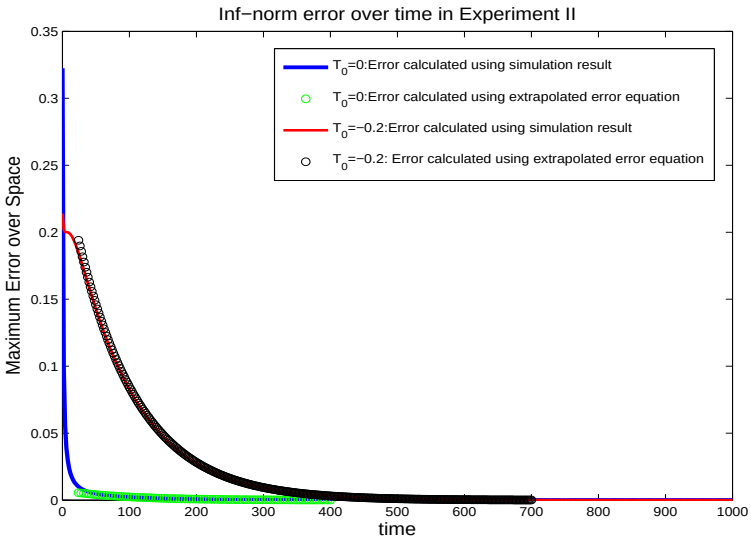

Figure 23: Experiment II: maximum error over time

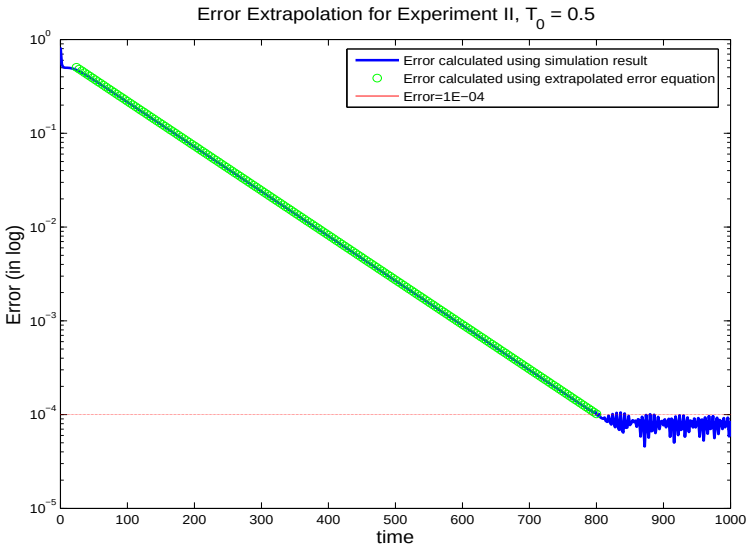

Figure 24: Model validation for Experiment II

5 Sensitivity Study on Hetergeneous Model

Error propagation in homogeneous model has shown high predictability from the study above. In reality, however, most of the soil environment is heterogeneous and thus a similar set of studies are done for a heterogeneous system.

Similar to procedures used in the previous study on homogeneous model, we first generate the true solution before we artifitially create solutions with false initial conditions. Since there is no analytical solutions for a heterogeneous model like the one described in Eq.(10), instead, the true solution is the numerical results of a specific scenario that we defined. We chose a non-uniform five layer soil structure described in Section 2.1. The five corresponding conductivity values are $0.1314, 0.2592, 0.1682, 0.3842,$ and 0.2822 (cm/min). The entire set up is identical to the 12-hour final-time study using 30cm as bottom depth and data as boundary and initial conditions. More details are given in Section 3.4 and the optimal results are also shown in Table 3. For this specific study, we set the simulation time as seven days to make full use of the seven day data as boundary condition.

5.1 Type I Error

This Type I Error for a heterogeneous system is defined similar to the homogeneous case (Eq.(12)):

$$T(z,0) = DATA(z,0) + \epsilon. \tag{23}$$

Here, $DATA(z,0)$ is the first row of the data set, describing initial temperature profile. The Es are chosen to be ± 4, $-6, -3, 9, 12$, approximately $\pm 10\%$ to $\pm 30\%$ of the mean temperature of 40^oC. Figure 25 compares the tweaked initial conditions with the original initial condition.

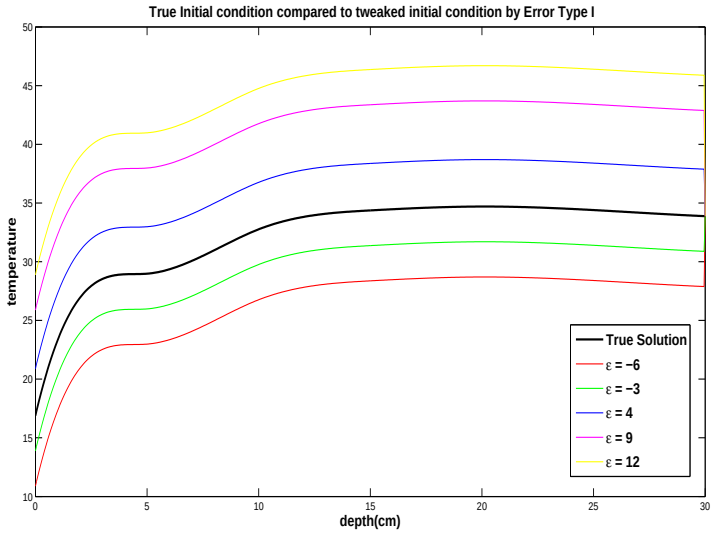

Figure 25: True initial condition compared to tweaked initial condition, Experiment I for Heterogeneous Model

5.1.1 Numerical Experiments

We simulate the solutions using the perturbed initial conditions for seven days. Error is calculated using infinity norm of the differences of two matrix. Figure 26 plots, in log scale, the infinity-norm error over time domain of 10800 minutes (7 days). Notice that the curve for $\epsilon = 4$ and $\epsilon = -4$ overlaps, indicating that the sign of error is insignificant to the propagation pattern. For simplicity, we omitted $\epsilon = -4$ in later experiments. Notice that this conclusion was obtained for the homogeneous model (Section 4) as well.

We also notice that, the magnitude of error does not converge to the truncation error as it did for homogeneous model (Section 4.1.1). This can be explained using the following reasoning: 1) the error from the heterogeneous study is calculated between two numerical estimations with the same finite difference setup; 2) since the finite difference setups are the same, the truncation error in both simulations should be close; 3) therefore, in the process of error calculation, the truncation errors from both numerical simulations cancel out. This explains the absence of a lower bound on the error in our heterogeneous study.

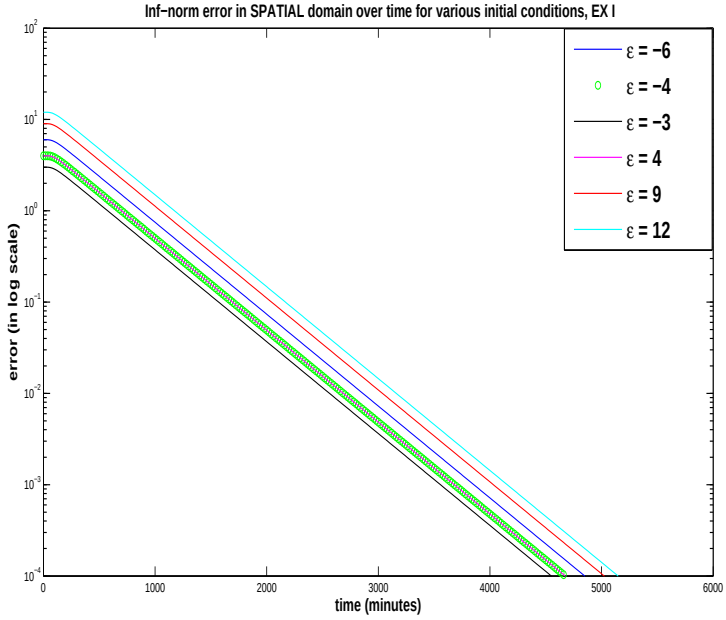

Figure 26: Infinity norm error over time, Experiment I, Heterogeneous Model

Figure 27 demonstrates how the simulations with tweaked initial conditions gradually approach the true solution. Notice that the difference becomes sufficiently small at the 33rd hour and the curves visually overlap.

5.1.2 Analysis and Error Function for Type I Error

The same linear pattern is found in the log plot of error in the heterogeneous model as was discovered for the homogeneous case. Here, we first calculate the rate of change of the log error using

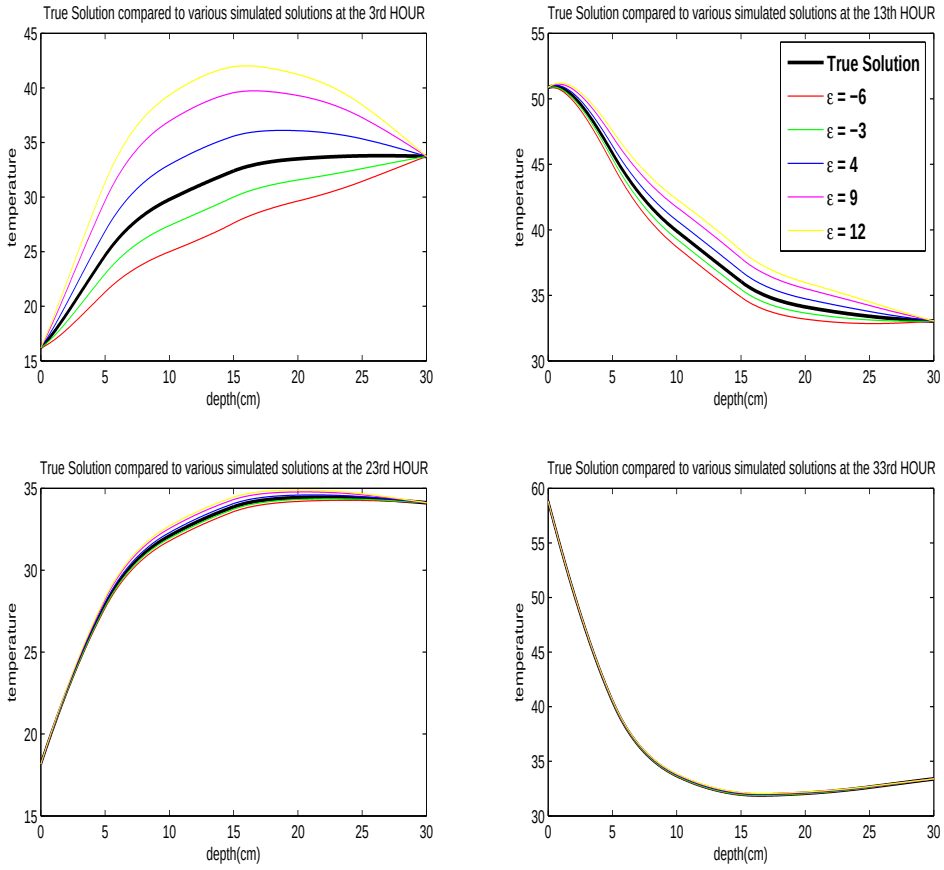

Figure 27: True solution compared to simulated solutions at various time for each ϵ, Experiment I

data fitting technique:

$$\frac{dlog(E_\epsilon)}{dt} \approx -0.0010 \tag{24}$$

The unit of this rate is $\frac{log(Error)}{time}$, since the linearity is shown in the log plot of error.

Next, we construct the line that describes the log of the error over time for different ϵ. Figure 26 shows that the curve stays flat at the beginning. Further data analysis confirmed that the error stays constant until the 100th minute for all ϵ tested in Experiment I. This implies that the linear error equation for each ϵ always passes through the point $(100, log(|\epsilon|))$. Now, we can formalize our analysis with the following:

$$log(E_\epsilon(t)) = -0.0010 \times (t - 100) + log(|\epsilon|), \tag{25}$$

where

$$\begin{aligned} E_\epsilon(t) &= 10^{-0.0010\times(t-100)+log(|\epsilon|)} \\ &= |\epsilon| \times 10^{-0.0010\times(t-100)}. \end{aligned} \tag{26}$$

To validate the above analysis, we present the following plots:

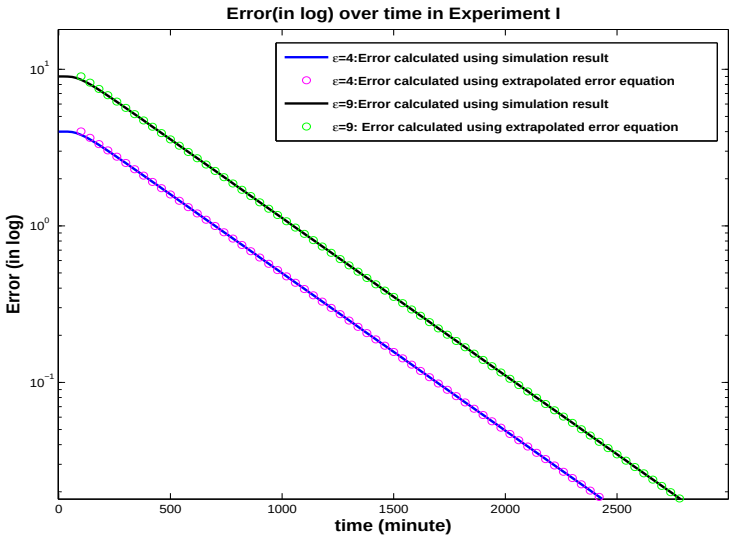

Figure 28: Heterogeneous Model Experiment I: log(error) over time

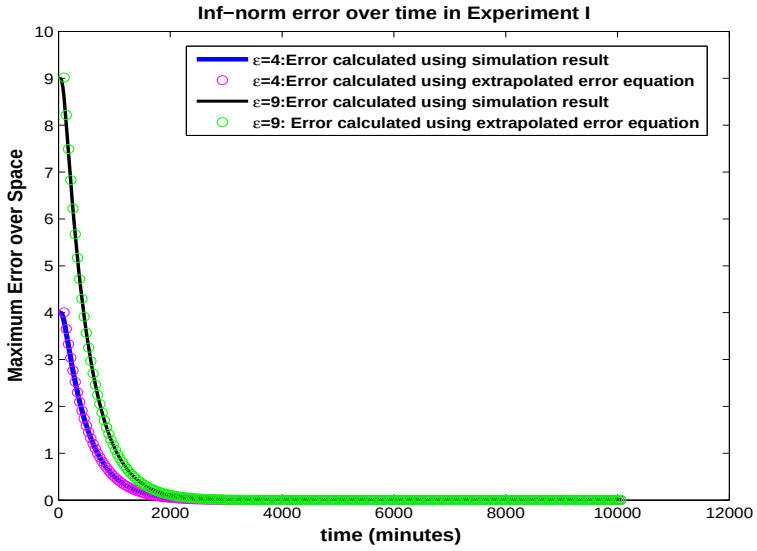

Figure 29: Heterogeneous Model Experiment I: maximum error over time

Figure 28 shows the original curve of $log(Error)$ over time for $\epsilon = 4$ and $\epsilon = 9$ in solid line; then the same curves are generated using Eq.(29) with the two different Es. Both graphs show good fitting between data and the predictions made by the equations. Further validation was done to confirm the correctness of Eq.(29); details are not given here due to its similarity to what was done in the homogeneous study. Figure 29 is the infinity norm error plotted over time using both data and Eq.(29).

5.2 Type II error

Type II error is the same as what was previously defined in Eq.(18) for homogeneous study:

$$T(z, 0) = T_0, \tag{27}$$

which says that the temperature is initially constant throughout the spatial domain. We ran five sets of experiments and for each set chose $T_0 = 20, 30, 40, 50, 60^oC$ respectively; here, the T_0s are chosen to be within the range of real data (13^oC to 67^oC). Figure 30 plots the tweaked initial conditions and the original initial condition.

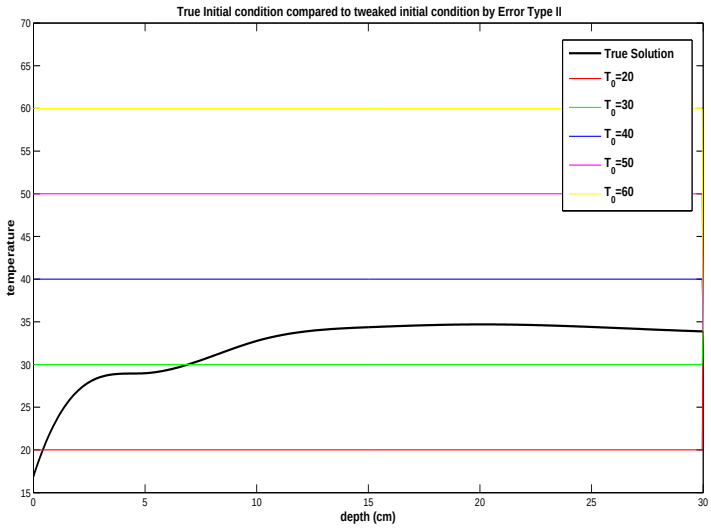

Figure 30: True initial condition compared to tweaked initial condition, Experiment II for Heterogeneous Model

5.2.1 Numerical Experiments

Figure 31 plots, in log scale, the infinity-norm error over time domain for the Type II Error. Same linear pattern is seen here and convergance to the truncation error is not observed.

Figure 32 shows how the impact of artifitially tweaked initial condition eventually dissipates over time and the difference between true and ill-conditioned solutions becomes trivial in the end. More specifically, the curves overlap after the 33rd hour.These results are similar to what was shown for Type I Error.

5.2.2 Analysis and Error Function for Type II Error

The analysis for Type II Error is similar to the analysis given in previous session. Surprisingly, the rate of decrease of log error is the same for Type II as it is for Type I:

$$\frac{dlog(E_{T_0})}{dt} \approx -0.0010 \tag{28}$$

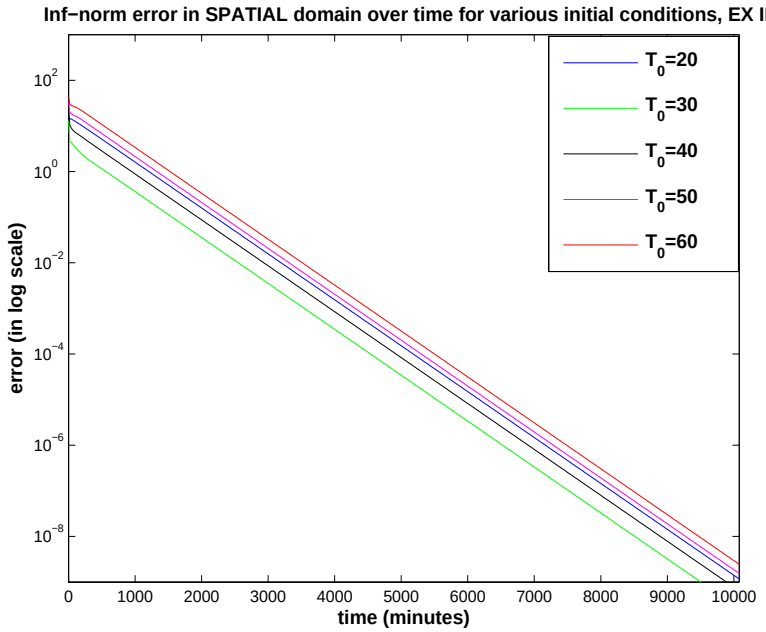

Figure 31: Infinity norm error over time, Experiment II, Heterogeneous Model

Next, using the same technique, we are able to construct the error function for Type II as the following:

$$\begin{aligned} E_{T_0}(t) &= 10^{-0.0010\times(t-100)+log(|\delta\, T_0|)} \\ &= |\Delta\, T_0| \times 10^{-0.0010\times(t-100)}. \end{aligned} \tag{29}$$

where $\Delta\, T_0$ is the temperature difference at the first time step, or the initial error:

$$\Delta\, T_0 = T_0 - DATA(0). \tag{30}$$

Validation of the above analysis is done similarly to what was shown in Type I error. Details will not be included here.

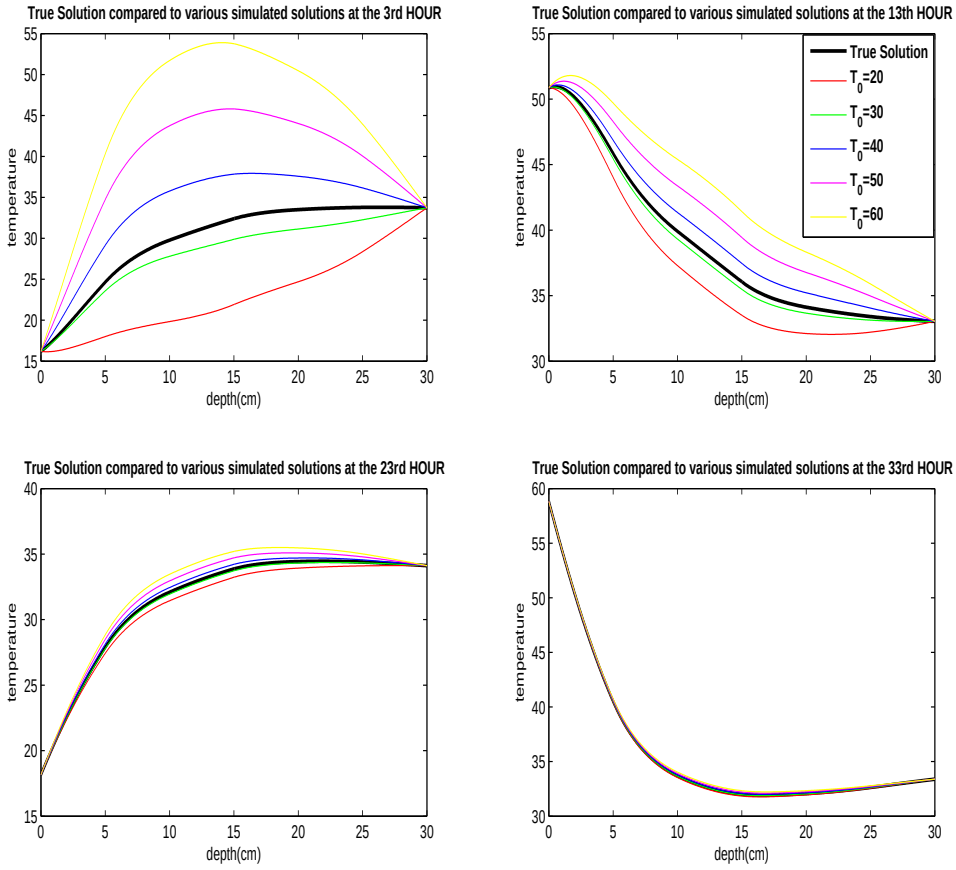

Figure 32: True solution compared to simulated solutions at various time for each T_0, Experiment II

6 Conclusion

For this work, we are given a data set that describes a subsurface soil temperature profile. To inversely map out the thermal conductivities that conrespond to the temperature data, we posed the work under an optimization framework where the objective is to minimize the error between simulation and data. The simulator solves the 1-D heat equation with heterogeneous K values. Specifically, the boundary conditions are implemented as Dirichlet conditions with values from data; the initial condition is implemented using recorded data as well.

A stable simulator is the key to a good conductivity estimation. The chanllenges of building a stable solver in this work come from the uncertainties within the given data set. Due to noises and unknown structures in the data, implementation details in the simulator can have significant impact on the results. The numerical experimentations in Section 3 gave us the opportunity to evaluate how choices on the simulation and optimization process impact the final solutions. Through these studies, we are able to decide on the optimal set up for a stable solver. With this solver, we are able to identify a set of thermal conductivities that simulates well-fitting temperature profile compared to the data at all times. The best identified optimal set of K values are shown in Table 10 (see also Table 7).

Table 10: Best identified K values

K_5	K_{10}	K_{15}	K_{20}	K_{25}	K_{30}	**nLSE**(Error)
0.1724	0.1579	0.2151	0.1988	0.2783	0.2242	4.0694e-006

The oscillation among these K values are small, indicating a potential homogeneous subsurface system.

To support the numerical and optimization work with data, we also conducted a sensitivity analysis on the simulator and its error propagation pattern. Both the optimization results from data and the analytical study confirmed that the initial error dissipates out of the system over time. We are also able to quantify the amount of time it takes for error to become insignificant in a system, if given the intial error.

References

[1] D. Powers, *Boundary Value Problems and Partial Differential Equations*, chapter 2, ELSEVIER Academic Press, 2006.

[2] T.N. Narasimhan, *The dichotomous history of diffusion,* Physics Today 62, 48, 2009.

[3] Z. Gao, L. Wang, and R. Horton, *A comparison of six algorithms to determine the soil thermal diffusivity at a site in the lowess plateau of China.,* Hydrology and Earth System Sciences Discussions, 6:2248-2274, 2009.

[4] R. Horton, P.J. Wierenga, and D. R. Nielson, *Evaluation of methods for determining the apparent thermal diffusivity of soil near the surface,* Hydrology and Earth System Sciences Discussions, 6:2248-2274, 2009.

[5] C. T. Kelley, *MATLAB/FORTRAN software for Iterative Methods for Optimization* http://www4.ncsu.edu/∼ctk/matlab_darts.html (online distribution), 1998

[6] D. E. Goldberg *Genetic Algorithms in Search, Optimization and Machine Learning* Addison-Wesley Longman Publishing Co., Inc., 1989